

ASSESSMENT OF LIQUID HYDROGEN-POWERED AIRCRAFT RANGE: A NOVEL BREGUET FORMULATION

Giuseppe Palaia[1], Karim Abu Salem[2], Alessandro A. Quarta[3] & Pedro D. Bravo-Mosquera[4]

[1]Department of Mechanical and Aerospace Engineering, Politecnico di Torino, Torino, Italy
[2]Department of Civil, Environmental and Mechanical Engineering, Università degli Studi di Trento, Trento, Italy
[3]Department of Civil and Industrial Engineering, University of Pisa, Pisa, Italy
[4]São Carlos School of Engineering, University of São Paulo (EESC / USP), São Carlos, SP, Brazil

Abstract

This paper presents a modified Breguet-type range formulation for liquid-hydrogen-powered aircraft, with explicit consideration of storage-related losses during cruise. The proposed approach couples a time-marching aircraft mission model with a low-order cryogenic tank model able to account for heat ingress, boil-off, ullage pressure rise, and venting. The reference application is a retrofitted short/medium-range transport aircraft equipped with an aft-fuselage liquid-hydrogen tank. A parametric campaign involving 5760 tank configurations is carried out by varying tank length, radius, insulation thickness, venting pressure, and initial fill factor. The resulting database is used to calibrate a power-law logarithmic surrogate model that introduces the effect of venting into the classical Breguet equation. The results show that neglecting venting systematically overestimates cruise range, especially for large tanks, long mission durations, and thin insulation. The proposed correction preserves the physical transparency of the classical Breguet formulation while significantly improving its predictive accuracy in this specific scenario. On the validation set, the mean absolute percentage error is reduced from 0.93% for the uncorrected Breguet-based equation estimate to 0.32% for the modified formulation, while the maximum error decreases from 13.68% to 1.62%. The proposed approach is therefore suitable for preliminary sizing and trade-off studies of liquid-hydrogen aircraft, where repeated coupled mission–tank simulations may be computationally inefficient.

Keywords: Liquid hydrogen, Breguet equation, aircraft range estimation, boil-off, surrogate modelling

1. Introduction

Reducing the climate impact of aviation is one of the main challenges for the next generation of aircraft. Improvements in aerodynamic efficiency, propulsion technology, lightweight structures, and flight operations can reduce fuel consumption, but they are not sufficient on their own to achieve the long-term emission-reduction targets expected for the aviation sector [1]-[6]. For this reason, alternative energy carriers are being investigated as possible enablers of a deeper transformation of aircraft design. Among them, hydrogen is receiving particular attention because it can be used without producing carbon dioxide during flight and because, on a mass basis, it stores much more energy than conventional kerosene[7]-[19].

Despite its high gravimetric energy density, hydrogen is difficult to integrate into aircraft because of its low density. Even in liquid form, it requires much larger storage volumes than kerosene and must be kept at cryogenic temperature, around 20 K, inside a fuselage tank. The hydrogen integration has direct consequences on tube-and-wing aircraft layout. In conventional aircraft, kerosene is usually stored inside the wing, with limited impact on the available cabin volume. This solution is generally not feasible for liquid hydrogen, as a result, liquid-hydrogen tanks are usually placed inside the fuselage, behind the passenger cabin, or in external pods, affecting payload capacity, fuselage arrangement, structural mass, aerodynamic drag, center-of-gravity position, and mission performance [13],[20]-[26]. To overcome the issues raised in the hydrogen tube-and-wing aircraft unconventional configurations such as blended-wing-body [27],[28], strut-braced-wing [29],[30], and

box-wing aircraft are investigated [31]-[33]. The potential breakthrough offered by unconventional aircraft configurations lies in their ability to exploit both alternative airframe layouts and configuration-specific functional or performance advantages, enabling a more effective integration of LH_2 tanks while mitigating the associated penalties in terms of mass, volume, and overall aircraft performance. These preliminary studies have shown that hydrogen can enable substantial environmental benefits but significant configuration changes and careful tank integration are to be considered since the initial design phases.

The tank is exposed to an external environment that is much warmer than the cryogenic fluid causing a heat flow toward the cryogenic side. This calls for insulated tanks, suitable materials, dedicated safety measures, and careful thermal management [13],[14],[34]-[36]. Although insulation reduces the heat flow, a certain amount of heat still reaches the liquid hydrogen and causes part of the liquid to evaporate, increasing the mass of hydrogen vapour in the ullage region and raising the internal pressure. When the pressure reaches the prescribed venting limit, gaseous hydrogen must be discharged to keep the tank within its allowable operating range [37],[38]. The vented hydrogen is lost from the aircraft and can no longer be used by the engines. Consequently, the initial mass of hydrogen loaded into the tank is not fully equivalent to the hydrogen mass available for propulsion. The amount of hydrogen lost through boil-off and venting depends on both tank design and mission duration. For instance, a larger tank can store more fuel and extend the cruise segment, but it also changes the heat-transfer surface and may allow venting losses to accumulate over a longer time. Several models have been developed to describe the thermal behaviour of liquid-hydrogen tanks. Low-order thermodynamic models are useful during conceptual design because they can estimate pressure evolution, boil-off, and venting with limited computational cost [37]-[44]. More detailed numerical methods, such as computational fluid dynamics and large-eddy simulation, can resolve local phenomena with higher fidelity, including stratification, phase change, and transient flow effects [45]-[47]. These methods are valuable for detailed design and safety analysis, but they are less suitable for early-stage aircraft studies, where many configurations must be evaluated repeatedly. For this reason, preliminary aircraft design requires formulations that are simple enough for rapid calculations, but still able to represent the dominant physical effects of hydrogen storage. In this respect, ref. [38] proposes its model as suitable for the conceptual design phase, claiming for fast and reliable results.

However, the integration of simple formulation for the conceptual design phase represents a milestone in the aircraft design process, where analytical formulation are useful to initialize the design process. In this, context, classical Breguet equation is widely used in aircraft conceptual design because it gives a compact relationship between cruise range, speed, aerodynamic efficiency, fuel consumption, and weight ratio. Its strength is its simplicity and physical transparency. However, the equation assumes that the fuel mass contributing to the aircraft weight reduction is used for propulsion. This assumption is reasonable for conventional kerosene aircraft, but it becomes incomplete for liquid-hydrogen aircraft where part of the stored hydrogen may be vented before it can be burned.

The objective of this work is to introduce a modified Breguet-type range formulation for liquid-hydrogen-powered aircraft that accounts for storage-related hydrogen losses during cruise. The purpose is not to replace detailed mission-tank simulations, but to use them as a reference database from which a compact correction for the Breguet range equation can be derived. The proposed approach lies in preserving the classical structure of the Breguet formulation while introducing the range penalty associated with liquid-hydrogen storage losses. In this way, the effect of venting is condensed into a single correction term, allowing rapid range estimates during preliminary aircraft design.

The paper is organized as follows. Section 3 describes the reference aircraft, the liquid-hydrogen tank model, the aircraft mass update, the mission simulation procedure, and the derivation of the surrogate-based range correction. Section 3 discusses the effect of the main tank parameters on vented mass, gravimetric index, cruise range, and energy-utilization indicators. The same section presents the modified Breguet formulation and evaluates its accuracy against the coupled mission-tank simulations. Finally, the conclusions summarize the main findings and outline the next developments of the proposed approach.

2. Methodology and mathematical model

The workflow combines a mission-performance module, a liquid-hydrogen tank model and an analytical range formulation. For each selected tank configuration, the aircraft cruise mission and tank thermodynamics are advanced together in time. The resulting database is then used to calibrate a compact surrogate model that corrects the Breguet range equation. Figure 1 summarizes this logic.

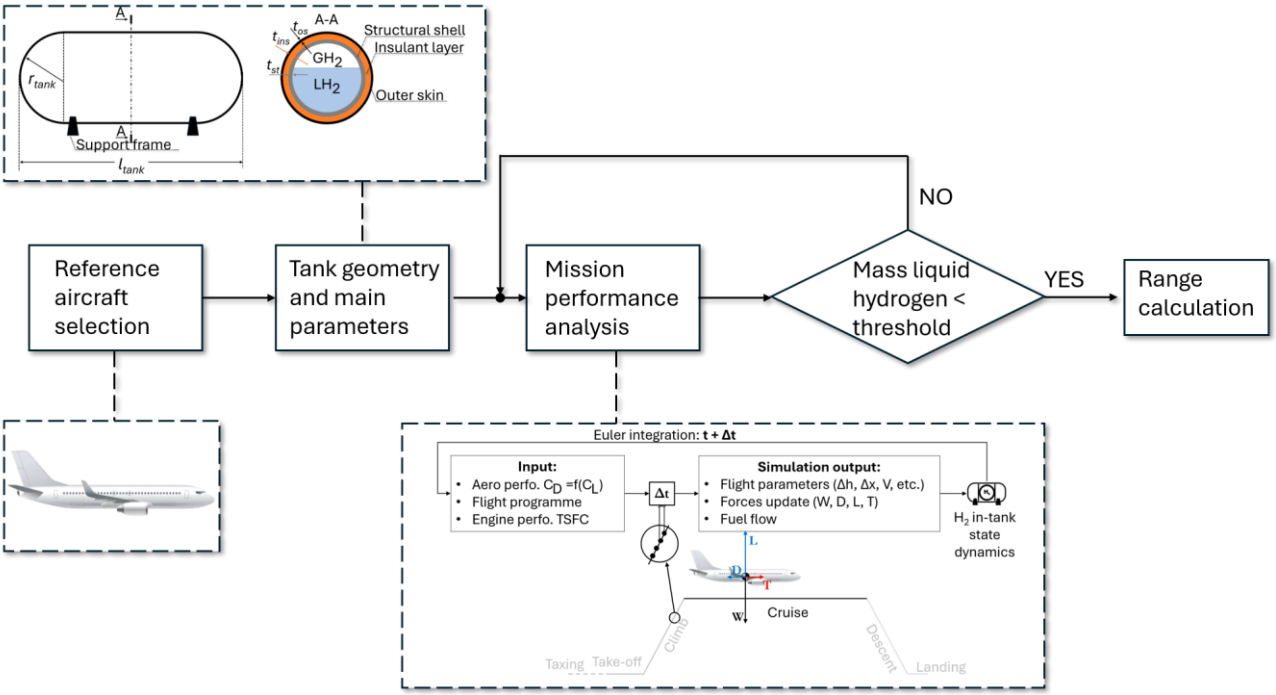


Figure 1 – Conceptual sketch of the workflow used to assess the range of an LH2-powered aircraft.

2.1 Simulation framework

The reference aircraft is the CeRAS short/medium-range twin-engine transport aircraft [48] whose data are reported in Table 1. The aerodynamic, propulsion and mass data are fixed at the beginning of each run of simulation so that the effect of the hydrogen tank can be isolated. The aerodynamic model is based on a parabolic drag polar, and the hydrogen turbofan is assumed to have a thermodynamic efficiency comparable to that of the kerosene baseline, consistently with the retrofit assumptions of Ref. [32]. The hydrogen thrust specific fuel consumption (TSFC) c_{LH2} is therefore scaled using the relative fuel-energy densities E_{ker}/E_{LH2}, and c_{ker} is the kerosene-based TSFC.

$$C_{LH2} = c_{ker} E_{ker} / E_{LH2} \tag{1}$$

Table 1 – Main data of the reference aircraft.

Category	Parameter	Symbol	Value	Unit
Geometry	Wing reference area [48]	S	122.4	m²
	Fuselage equivalent diameter [48]	d_f	4	m
	Wingspan [48]	b	34	m
	Fuselage length [48]	l_f	37.5	m
Mass	Operating Empty Weight [49]	W_{oe}	42054	kg_f
	Maximum Take-Off Weight [49]	W_{max}	77000	kg_f
	Number of passengers	n_{pax}	186	-
Aerodynamics	Zero-lift drag coefficient [49]	C_{D0}	0.0171	-
	Coefficient quadratic term polar drag [49]	k	0.0598	-
Propulsion	Kerosene-based TSFC [49]	c_{ker}	0.50	1/h
	LH_2 TSFC (Eq. (1))	c_{LH2}	0.18	1/h
	Energy density kerosene [13]	E_{ker}	12	MWh
	Energy density LH_2 [13]	E_{LH2}	33	MWh

2.2 Liquid-hydrogen tank model

The storage system is represented by a non-integral cylindrical tank with hemispherical end caps installed in the aft fuselage and connected to the fuselage through the support frame. The tank includes an inner load-bearing shell, a foam insulation layer and a thin outer skin to protect the insulation layer and the hydrogen from contamination. Its internal volume is divided into a liquid region and an ullage region, whose relative sizes vary during the mission as fuel is consumed, boil-off occurs and venting events are triggered. Figure 2 shows the adopted geometry, while Table 2 summarizes the main design parameters.

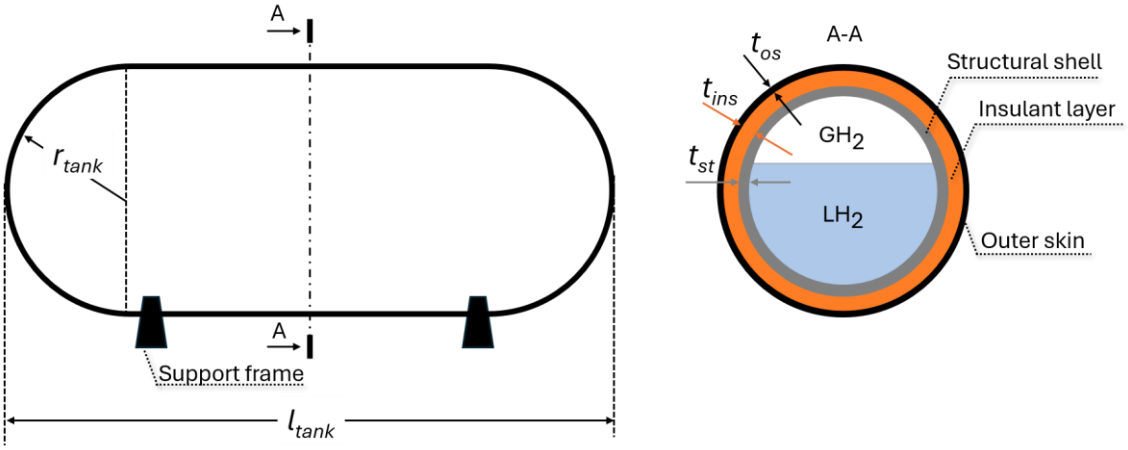


Figure 2 - Schematic representation of the liquid-hydrogen tank.

The design variables are tank length, tank radius, insulation thickness, venting pressure and initial fill factor whose bounds are reported in Table 2. Tank length and radius (the distance between the external side of the skin and the center of the hemispherical part) define the storage capacity and the heat-transfer area; insulation thickness controls heat ingress; venting pressure sets the threshold for gas discharge; and fill factor fixes the initial liquid/ullage split. The venting-pressure range is kept above 1.45 bar to preserve an overpressure margin against air ingress in cryogenic operation.

Table 2 – Main data of tank parameters.

Category	Parameter	Symbol	Material	Value	Unit
Geometry	Tank length	l_{tank}	–	[5, 12]	m
	Tank radius	r_{tank}	–	[0.75, 2]	m
	Insulation thickness	t_{ins}	Polystyrene foam	[20, 220]	mm
	Outer skin thickness [50]	t_{os}	Aluminium Alloy 2219	1.6	mm
Thermodynamics	Venting pressure	P_v	–	[1.59, 2.75]	bar
	Initial fill factor	f_f	–	[0.8, 0.95]	-
	Minimum internal pressure [51],[52]	P_{min}	–	1.45	bar

The thickness of the inner load-bearing shell is obtained through a preliminary iterative structural sizing procedure based on the ASME Boiler and Pressure Vessel Code [53]. Hereafter a brief overview is presented, for more details the reader can refer to [32]. For each tank geometry, the procedure first computes the wall thickness required to withstand the internal design pressure. The sizing pressure is assumed equal to two times the venting pressure, so that a safety factor of 2 is applied. This value resembles recent LH2 aircraft studies [50], although lower values are also used in the literature [54]. In this step, the cylindrical shell is sized by considering both hoop and longitudinal stress conditions, including the material allowable stress, the weld efficiency, and the minimum thickness prescribed by the code. The end caps are sized in a similar way by applying the corresponding pressure-vessel relations. After this first pressure-driven estimate, the tank mass and internal volume are updated. The mass of the metallic shell, the insulation layer, and the stored liquid hydrogen are then used to define the longitudinal mass distribution of the tank. This distribution is

required to estimate the bending moment between the support frames (cf. Figure 2) and the axial inertial loads associated with the prescribed flight load factors. The cylindrical shell is therefore checked not only against tensile stress, caused by the combined effect of internal pressure and bending, but also against compressive instability. In particular, the local wall-buckling limit is evaluated according to the formulation described in [53]. If either the tensile-stress verification or the buckling verification is not satisfied, the cylindrical shell thickness is increased and the tank mass, internal volume, bending moment, inertial loads, and stress state are recalculated. The loop is repeated until all structural checks are fulfilled. In this way, the final shell thickness accounts not only for internal pressurization, but also for the coupling between tank geometry, structural mass, stored hydrogen mass, support spacing, and inertial loads. The mass of the tank system is then assembled from the masses of the outer skin, structure and insulation, plus the initial liquid-hydrogen mass.

2.3 Aircraft mass update and simplified mission analysis

The retrofit method follows the methodology described in Ref. [32]. The baseline structure and outer aerodynamic shape are kept unchanged, while the tank length affects the fuselage length available for passengers and containers which are recalculated accordingly. Passenger, baggage and container masses are then updated, and cabin-dependent systems and operating items are recomputed using the same statistical correlations adopted in Ref. [32]. The hydrogen retrofit also includes the mass increase associated with the engine heat exchanger [55]. Regarding the aircraft mission, the cruise phase alone is simulated in this work. The simulation of the cruise phase is performed through a time-marching integration, where the aircraft equations of motion and the cryogenic tank thermal model are solved simultaneously at each time step Δt, for more details the reader can refer to Ref.s [31],[32]. The time evolution of the system is computed using the forward Euler method. Three hypotheses are assumed to model aircraft mission: (i) aircraft is modelled as a point mass, (ii) quasi-steady flight conditions, meaning that accelerations are negligible over each integration step, (iii) the motion is confined to the vertical plane, as a direct consequence, lateral dynamics is not considered. (iv) cruise climb, i.e. lift coefficient and speed are constant during the cruise phase. Accordingly, lift L and thrust T are equal to weight W and drag D, respectively.

At each time step, the mission module computes lift, drag and fuel flow $\dot{W}_{LH2}$ (computed by Eq. (2)), while the tank module computes heat ingress through convection, radiation and conduction across the insulation. The added heat evaporates part of the liquid hydrogen, increases ullage mass and raises tank pressure. If the pressure exceeds the venting pressure, gaseous hydrogen is vented until the allowable pressure is recovered. Eq. (3) computes the aircraft weight, where $\dot{W}_{vent}$ is the venting mass, computed according to the methodology described in [32].

$$\dot{W}_{LH2} = c_{LH2} T \tag{2}$$

$$\dot{W} = \dot{W}_{LH2} + \dot{W}_{vent} \tag{3}$$

The mission simulation stops when the remaining liquid level reaches 10% of its initial height. This threshold is introduced as a conservative residual-liquid condition: the model does not assume that the tank can be completely emptied, since the last fraction of liquid hydrogen may not be reliably extracted or may be kept as an operational safety margin. The initial conditions of the simulations are cruise altitude equal to 11 km, cruise Mach equal to 0.8 and pressure of the ullage equal to 99% of the venting pressure, this value has been selected in order to have an internal pressure close to the venting without forcing it. The venting is then assessed trough the tank simulation.

2.4 Surrogate modelling and range formulation

The objective of the surrogate model is to derive a compact correction of the Breguet range equation from the database generated by the coupled mission-tank simulations. The surrogate model is therefore not used to predict the aircraft range directly, but to estimate a dimensionless range-penalty factor that accounts for hydrogen losses associated with boil-off and venting. This choice preserves the physical meaning of the classical Breguet formulation and introduces the tank-related losses through a single correction term.

For each tank configuration, the simulation workflow provides the cruise range obtained from the

time-marching mission analysis, denoted as R_{sim}, together with the initial aircraft mass, the initial amount of liquid hydrogen stored in the tank, the cruise speed, the average aerodynamic efficiency, and the hydrogen thrust specific fuel consumption. A reference Breguet range R_B is first computed without explicitly accounting for venting losses

$$R_B = \frac{V(L/D)}{c_{LH2}} log\left(\frac{M_0}{M_0 - k_{LH2} m_{LH2,0}}\right) \tag{4}$$

where V is the cruise speed, (L/D) is the aerodynamic efficiency during cruise, M_0 is the aircraft weight at the beginning of cruise, $m_{LH2,0}$ is the liquid hydrogen mass stored in the tank at the beginning of the mission, k_{LH2} is the usable-fuel coefficient. In the present implementation, k_{LH2} is equal to 0.965, consistently with the threshold value adopted to stop the simulation (cf. Figure *1*).
Eq. (4) overestimates the mission-simulated range because it assumes that the available hydrogen contributes only to propulsion. In the coupled simulation, part of the hydrogen can instead be lost through venting after boil-off and pressure build-up inside the tank. The difference between the analytical R_B and simulated R_s ranges is therefore used to define a target equivalent-consumption multiplier μ bigger than one and defined as

$$\mu = R_B/R_s \tag{5}$$

If μ is equal to one, the uncorrected Breguet formulation reproduces the simulated range, If μ is greater than one, the uncorrected Breguet formulation, i.e. Eq. (4), overestimates the simulated range and an equivalent increase in fuel consumption is required. The modified Breguet equation is then written as follow

$$R_{B,m} = \frac{V(L/D)}{\hat{\mu}\, c_{LH2}} log\left(\frac{M_0}{M_0 - k_{LH2} m_{LH2,0}}\right) \tag{6}$$

where $\hat{\mu}$ is the value predicted by the surrogate model. The correction can therefore be interpreted as an equivalent increase in the thrust specific fuel consumption caused by venting. This coefficient is expected to be greater than one, so the correction factor can be defined as the sum of a constant term equal to one and a term, which has to be positive, depending on tank size. The correction factor can be expressed by Eq. (7) where the exponential term $\hat{\eta}$ has been introduced to guarantee a second positive addendum.

$$\hat{\mu} = 1 + exp(\hat{\eta}) \tag{7}$$

$\hat{\eta}$ is written as a function of the function of the vector of the design variables $\boldsymbol{x} = (x_1,\ldots,x_n)$, where n is the number of the design variables. In this paper, n is equal to 5, and the tank design variables are tank length, tank radius, insulation thickness, venting pressure, and the fill factor. First, each design variable is normalized with respect to a reference value and then transformed into a logarithmic variable z_i

$$z_i = log\,(x_i / x_{i,ref}) \tag{8}$$

where x_i is the i-th design variable, and $x_{I,ref}$ is the corresponding reference value. The reference values $x_{I,ref}$ are selected as the medium value of the bounds of the design intervals reported in Table 2. The use of logarithmic design variables is adopted to describe the effect of the tank parameters in terms of relative variations with respect to their reference values. This is useful because the design variables have different physical units and different ranges of variation, and their effect on the range penalty is expected to depend more on proportional changes than on absolute changes. For instance, doubling a tank parameter and halving it with respect to the reference value produce logarithmic variations with the same magnitude and opposite sign. This property provides a balanced representation of variations above and below the reference condition. The variable $\hat{\eta}$ is then approximated through a multivariate polynomial model according to Eq. (9):

$$\hat{\eta}=a_0\times\sum_{i=1}^{n}a_i z_i\times\sum_{i\le j}^{n}a_{ij}z_i z_j\times\sum_{i=1}^{n}a_{ijk}z_i z_j z_k\times\sum_{i=1}^{n}a_{ijkl}z_i z_j z_k z_l \tag{9}$$

Eq. (9), which is a general formulation, includes a constant term a_0, linear contributions a_I, second-order interaction terms a_{ij}, third-order terms a_{ijk}, and fourth-order terms a_{ijkl}. In the model proposed in this formulation we considered only constant term, linear contributions and second-order interaction terms and we verified a-posteriori the goodness of the proposed formulation. According to the above discussion, and combining Eq.s (7-9), the correction factor can be expressed as

$$\hat{\mu}=1+\exp\left(a_0+\sum_{i=1}^{n}a_i\log\left(\frac{x_i}{x_{i,ref}}\right)+\sum_{i\le j}^{n}a_{ij}\log\left(\frac{x_i}{x_{i,ref}}\right)\log\left(\frac{x_j}{x_{j,ref}}\right)\right) \tag{10}$$

The coefficients of Eq. (10) are directly related to sensitivity meaning, indeed each coefficient indicates how strongly the range penalty changes when the corresponding design variable is varied in relative terms. For example, a positive coefficient means that increasing that variable tends to increase the equivalent consumption penalty, whereas a negative coefficient means that increasing the variable tends to reduce it. Therefore, the fitted coefficients help identify which tank parameters are most responsible for the deviation between the classical Breguet range and the simulated range. Considering the tank design variables, Eq. (10) can be rewritten as follows

$$\hat{\eta}=a_0+a_l\log\left(\frac{l_{tank}}{l_{tank,ref}}\right)+a_r\log\left(\frac{r_{tank}}{r_{tank,ref}}\right)+a_t\log\left(\frac{t_{ins}}{t_{ins,ref}}\right)+a_p\log\left(\frac{P_v}{P_{v,ref}}\right)+a_{ff}\log\left(\frac{f_f}{f_{f,ref}}\right)+\sum_{i\le j}^{n}a_{ij}x_i x_j \tag{11}$$

$$\begin{aligned}\sum_{i\le j}^{n}a_{ij}x_i x_j=&a_{lt}\log\left(\frac{l_{tank}}{l_{tank,ref}}\right)\log\left(\frac{t_{ins}}{t_{ins,ref}}\right)+a_{rp}\log\left(\frac{r_{tank}}{r_{tank,ref}}\right)\log\left(\frac{P_v}{P_{v,ref}}\right)+a_{tp}\log\left(\frac{t_{ins}}{t_{ins,ref}}\right)\log\left(\frac{P_v}{P_{v,ref}}\right)\\&+a_{lp}\log\left(\frac{l_{tank}}{l_{tank,ref}}\right)\log\left(\frac{P_v}{P_{v,ref}}\right)\end{aligned} \tag{12}$$

where $l_{tank,ref}$, $r_{tank,ref}$, $t_{ins,ref}$, $P_{v,ref}$ and $f_{f,ref}$ are the corresponding reference value. The coefficients of the surrogate model are identified by minimizing the discrepancy between the modified Breguet range and the range obtained from the coupled mission-tank simulations. The dataset, whose bounds are defined in Table 2, is divided into a calibration subset and a validation subset. The calibration subset is used to estimate the coefficients, whereas the validation subset is used only to assess the predictive capability of the proposed formulation. The coefficients are found through an optimization problem, which exploits local algorithm, and minimizes the mean squared relative range error:

$$\mathrm{J}(\boldsymbol{x})=\frac{1}{N_{cal}}\sum_{i=1}^{N_{cal}}\left(\frac{R_{B,m,i}-R_{s,i}}{R_{s,i}}\right)^2 \tag{13}$$

where N_{cal} is the number of configurations in the calibration subset. This figure of merit is dimensionless and gives comparable weight to short- and long-range configurations because the error is normalized by the simulated range. Minimizing J therefore directly improves the accuracy of the range formulation, which is the final objective of the surrogate model.

3. Results

The results section is organized into two main parts. Section 3.1 discusses the effect of the tank design variables on the main performance indicators, including vented mass, gravimetric index, cruise range, and energy utilization. More specifically, a vector of discrete values for each design variable has been defined allowing to evaluate 5760 different combinations. Section 3.2 then presents the surrogate-based correction of the Breguet range formulation and assesses its accuracy

with respect to the coupled mission-tank simulations

3.1 Parametric analysis

Figure 3 presents a 3×3 set of contour maps of the total vented hydrogen mass during cruise, plotted in the (l_{tank}, t_{ins}) plane. Each map represents a family of tank configurations generated within the simulation framework described in Sections 2.1-2.3, while the parameters held fixed in each panel vary across the grid: the tank radius increases along the columns, whereas the venting pressure increases along the rows. The first result is a monotonic decrease in m_{vent} with increasing t_{ins}: a thicker insulation layer increases the overall thermal resistance, thereby reducing heat transfer from the surroundings through the outer skin and insulation; the lower heat ingress reduces liquid evaporation, slows ullage pressure build-up, and consequently decreases the cumulative amount of hydrogen discharged through the vent system during cruise. The second result is the increase of m_{vent} with l_{tank}.

The rise in total vented mass is explained by the larger amount of hydrogen onboard, which extends cruise duration and allows the cumulative effects of boil-off and venting to develop over a longer time. A similar competition explains the column-wise trend: although increasing radius reduces surface-to-volume ratio, the figure indicates that the associated increase in absolute tank size and stored fuel mass dominates, leading overall to higher vented mass. Finally, increasing venting pressure shifts the contour levels towards lower values because the tank can tolerate a higher internal pressure before discharge occurs, thus delaying vent opening and reducing the total mass expelled over the mission.

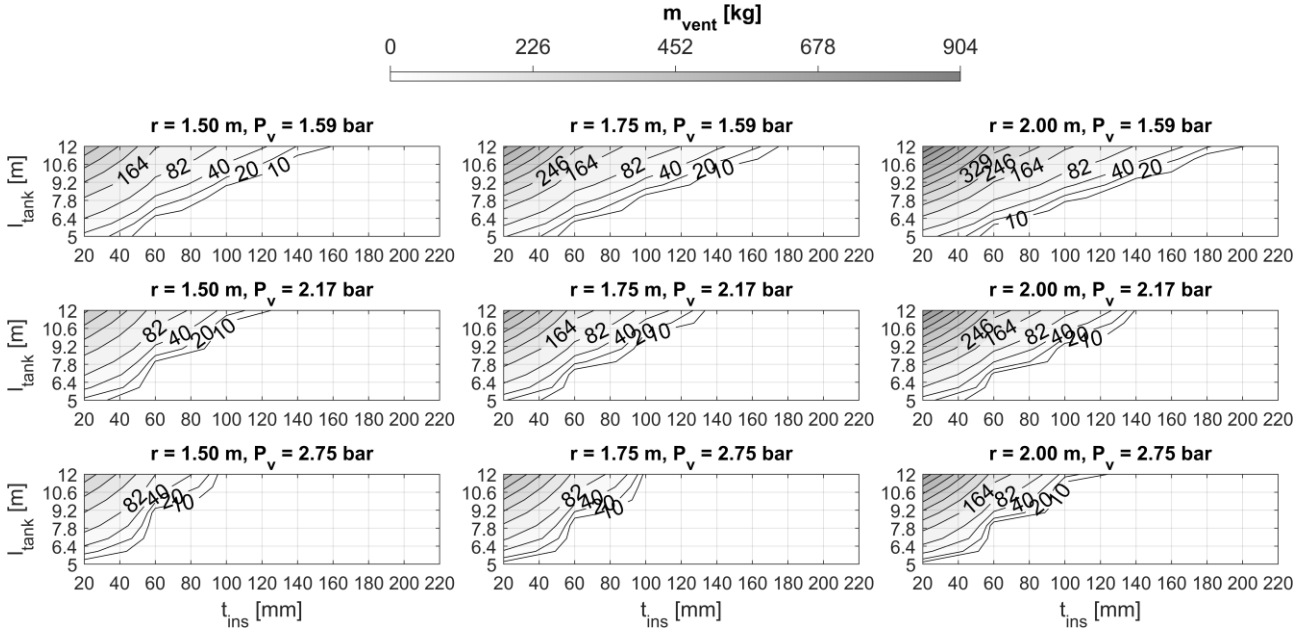


Figure 3 – l_{tank} versus t_{ins} contour maps of m_{vent} for different radii and venting pressures; f_f = 0.9.

Figure 4 presents a 3×3 set of contour maps of the tank-system gravimetric index GI defined as the ratio of the hydrogen mass stored in the tank at the beginning of the mission and the tank total mass. As well known, GI quantifies the mass efficiency of the storage system, namely the fraction of the overall tank-system mass that is represented by usable liquid hydrogen. The contour maps show that GI generally increases with tank length and decreases with insulation thickness. Increasing the length of the tank improves GI because, when the tank is elongated at fixed radius, the internal volume and therefore the storable hydrogen mass increase more rapidly than the associated increase in structural mass. As a result, the fraction of fuel mass within the overall tank-system mass becomes larger. However, the maps also show that this trend depends on venting pressure. In particular, for venting pressure equal to 1.59 bar, an excessive increase in length eventually leads to a reduction in GI. This behaviour can be explained by the structural sizing model, which also accounts for buckling: beyond a certain length, buckling becomes relevant and requires an increase in structural thickness, so the structural mass rises more markedly and the gravimetric efficiency

deteriorates. At higher venting pressure, this effect is no longer observed because the dominant sizing load is the internal pressurization, and the buckling-driven thickness increase does not become active. Increasing insulation thickness reduces GI because a thicker insulation layer occupies a larger portion of the available tank envelope, leaving less volume for hydrogen storage. Increasing venting pressure also reduces GI, since a higher venting pressure implies a higher design pressure and therefore a larger required structural thickness. By contrast, the effect of the radius is weak: increasing the radius raises the pressurized-driven structural stresses and thus the structural mass, but it also increases the amount of hydrogen that can be stored. In the present results, these two effects nearly compensate each other, leading to very similar GI values across the different radii, as also shown by the data in Table 3.

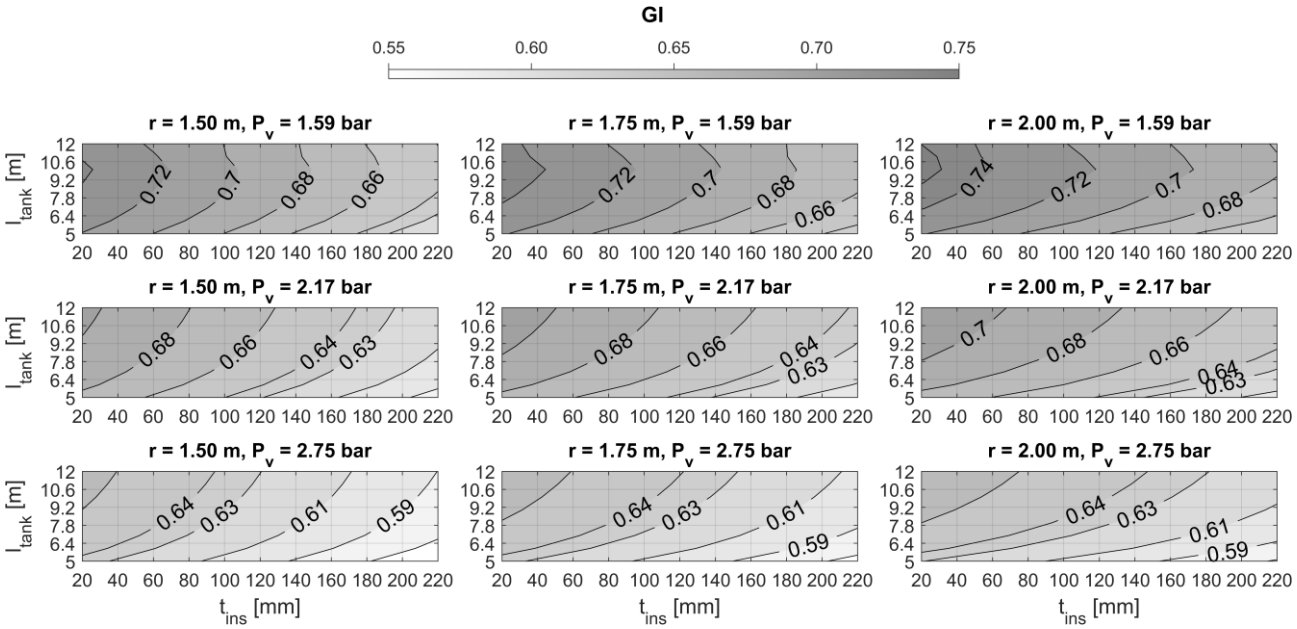


Figure 4 – l_{tank} versus t_{ins} contour maps of *GI* for different radii and venting pressures; f_f = 0.9.

Figure 5 and Figure 6 should be interpreted jointly, since they describe, respectively, the cruise range obtained from the mission simulations and the discrepancy introduced when the same configurations are evaluated through a Breguet-type range estimate that does not explicitly account for venting losses. The simulated range R_s shown in Figure 5, increases primarily with tank size, since increasing length and radius allows a larger storage of hydrogen and therefore a longer cruise segment before the mission stopping criterion is reached. By contrast, increasing the insulation thickness produces a slight reduction in range in most of the map, indicating that the reduction of internal volume to store hydrogen with thicker insulation is not fully compensated by the reduction in venting losses. The effect of venting pressure is more limited, but the maps suggest a slight decrease in range as increases, consistently with the heavier tank structure required by a higher design pressure, which slightly reduces the internal volume available for storage.
Figure 6 reports the corresponding percentage deviation ΔR between the simulated range and the value predicted by the Breguet formulation calculated according to Eq. (4).

$$\Delta R=(R_B - R_s)/R_s \tag{14}$$

The main result is that neglecting venting leads to non-negligible range deviations and systematically causes an overestimation of cruise range in the Breguet-based prediction. This effect becomes increasingly important for long-range configurations. In particular, ΔR is largest for long and large tanks combined with thin insulation, i.e. for the configurations that also exhibit the highest venting losses. In these cases, the mission duration is longer and the cumulative hydrogen mass discharged during cruise becomes more significant; if this loss mechanism is omitted from the analytical estimate, the predicted range departs appreciably from the simulated one. Conversely, increasing insulation thickness tends to reduce ΔR , because thicker insulation mitigates heat ingress and

therefore limits venting losses. A higher venting pressure reduces venting, but this does not produce a clear reduction in Δ*R*. The reason is that a higher venting pressure requires slightly reduced the range, and the percentage error remains approximately the same even if the vented mass is lower.

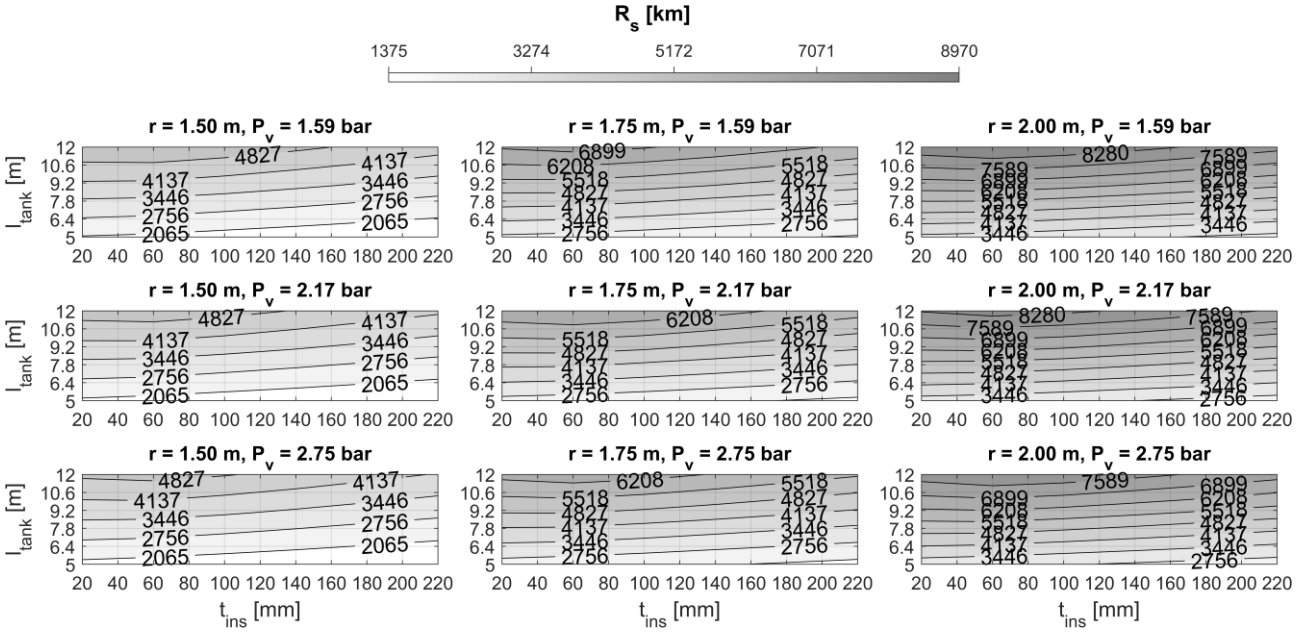


Figure 5 – l_{tank} versus t_{ins} contour maps of R_s for different radii and venting pressures; f_f = 0.9.

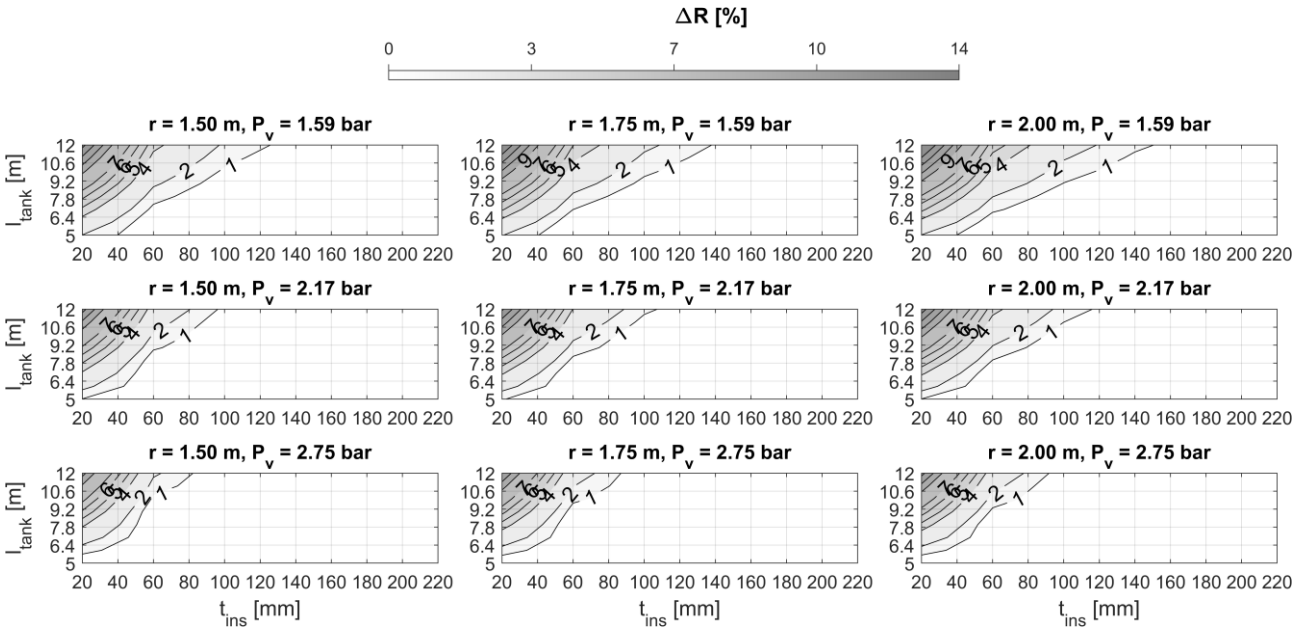


Figure 6 – l_{tank} versus t_{ins} contour maps of Δ*R* for different radii and venting pressures; f_f = 0.9.

Figure 7 shows the contour maps of a new performance indicator, the Propulsive Energy Utilization Factor Ψ, defined according to Eq. (13).

$$\Psi = E_m/E_{LH2,0} \tag{15}$$

Ψ is defined as the ratio between the energy spent to fly E_m and the chemical energy stored in liquid hydrogen at departure $E_{LH2,0}$. This factor measures the fraction of the initial stored energy in the tank actually exploited for propulsion, so it inherently accounts for venting losses, and it represents a metric for the efficiency of the overall propulsion system (engine and tank). Lower values means that the propulsion system loses energy due to boil-off and venting in the tank. Figure 7 shows that Ψ generally increases with insulation thickness and shorter tanks. This behaviour is physically

consistent with the definition of Ψ, since configurations that reduce venting losses allow a larger fraction of the initially stored chemical energy to be effectively converted into propulsive work during cruise. A similar, although weaker, effect is observed when venting pressure increases: a higher venting pressure delays gas discharge and reduces the vented mass, so a slightly larger fraction of the onboard energy is retained for propulsion. By contrast, the effect of tank radius on Ψ is limited. Increasing the radius increases the amount of hydrogen stored at the beginning of the mission, and therefore the initial chemical energy available onboard, but it also enables a longer cruise segment and thus a larger amount of energy spent for flight. In the present results, these two effects vary in a similar way, so Ψ remains nearly unchanged, with only a slight decrease visible in Table 3. From a design standpoint, these maps also highlight a trade-off. If Ψ is improved by increasing insulation thickness or venting pressure, the tank becomes thermodynamically more efficient, but the aircraft range tends to decrease because thicker insulation and higher-pressure structural sizing penalize the available storage volume. Therefore, reducing storage-related losses does not automatically maximize aircraft performance, and the final design must balance propulsive energy utilization against achievable range.

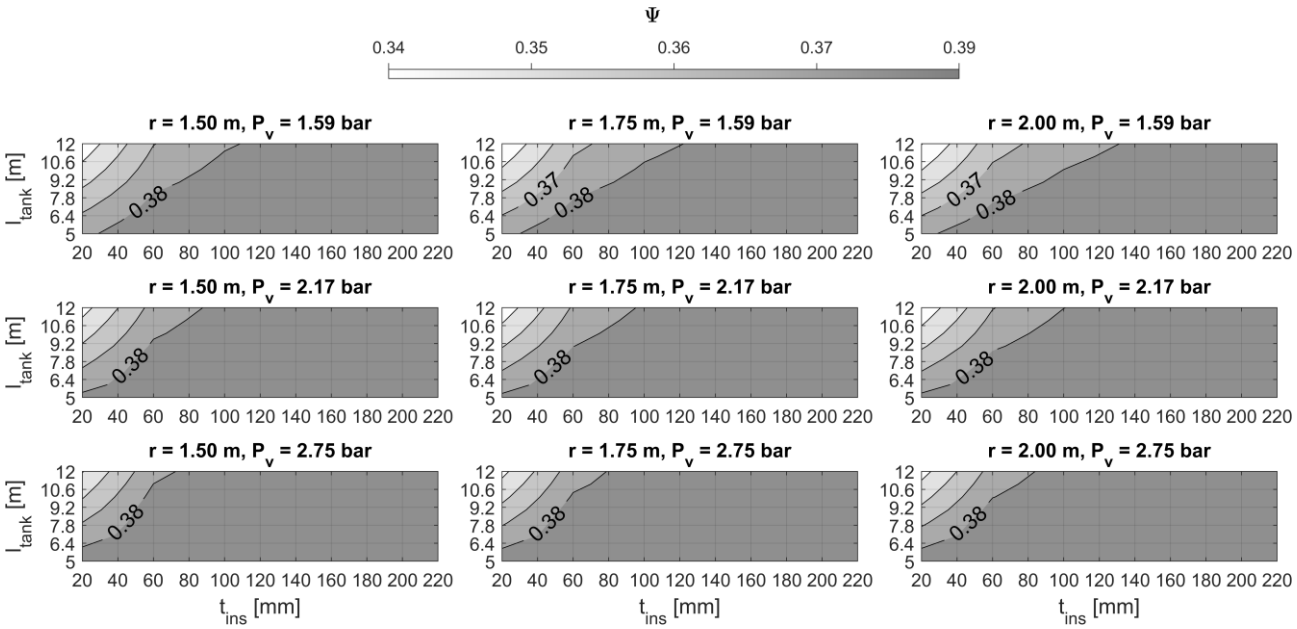


Figure 7 – l_{tank} versus t_{ins} contour maps of Ψ for different radii and venting pressures; f_f = 0.9.

Table 3 – Data of 9 configurations varying the design variables.

	Case 1	Case 2	Case 3	Case 4	Case 5	Case 6	Case 7	Case 8	Case 9
f_f	0.9	0.9	0.9	0.9	0.9	0.9	0.9	0.9	0.9
r [m]	1.5	1.75	2	1.5	1.75	2	1.5	1.75	2
P_v [bar]	1.59	1.59	1.59	2.17	2.17	2.17	2.75	2.75	2.75
l_{tank} [m]	11	11	11	11	11	11	11	11	11
t_{ins} [mm]	60	60	60	60	60	60	60	60	60
m_{vent} [kg]	103	203	290	90	148	215	51	93	142
m_{LH2} [kg]	3580	4834	6241	3488	4708	6078	3407	4588	5938
$t_{tank,st}$ [mm]	3.3	3.9	4.4	4.3	5	5.8	5.4	6.4	7.3
$m_{tank,st}$ [kg]	914	1258	1657	1191	1640	2162	1508	2078	2738
m_{tank} [kg]	1546	1996	2501	1823	2378	3006	2140	2816	3582
GI	0.72	0.73	0.74	0.69	0.69	0.70	0.65	0.66	0.66
Ψ [%]	37.2	37.0	36.9	37.6	37.4	37.3	38.0	37.8	37.7
R_s [km]	4931	6512	8192	4759	6261	7837	4600	6010	7507
R_B [km]	5110	6787	8573	4882	6458	8116	4670	6133	7687
ΔR [%]	3.64	4.23	4.66	2.60	3.15	3.55	1.51	2.04	2.41

3.2 Surrogate model

This section presents the assessment of the modified Breguet formulation obtained through the surrogate-model procedure described in Section 2.4. The calibration and validation sets are composed of 4608 and 1152 random combinations, respectively; accordingly, the calibrated coefficients of the range-penalty model are reported in Table 4.

Table 4 – Data of optimum coefficients for Breguet modified equation.

	a_0	a_l	a_r	a_t	a_p	a_{ff}	a_{lt}	a_{rp}	a_{tp}	a_{lp}
Coeff.	-3.404	1.153	0.345	-0.602	0.341	0.669	-0.147	-0.146	0.137	-0.177

The signs and magnitudes of the fitted coefficients should be interpreted together with the parametric trends discussed in Section 3.1. For example, the coefficient associated with insulation thickness is expected to be negative, because a thicker insulation layer reduces heat ingress, slows down boil-off, delays pressure build-up, and limits venting. Conversely, the coefficient associated with tank length may become positive if the longer available cruise duration allows storage-related losses to accumulate over a longer time.

The performance of the corrected formulation is evaluated by comparing three quantities: R_s, R_B, and $R_{B,m}$. Figure 8-left reports the parity plot, i.e. chart which compares simulated data and predicted data, between R_s and the range predicted by the analytical formulations R_p according to Eq.s (4,6). The ideal result corresponds to the one-to-one line, i.e. when the predicted data exactly correspond to the simulated ones. Points above this line indicate range overprediction, while points below this line indicate range underprediction. The results shows that, as expected, the results of R_B are above the ideal line, whereas the results of $R_{B,m}$ resembles the ideal line, meaning that the proposed formulation allows to better predict the range. For $R_{B,m}$, the percentage has been calculated as in the Eq. (12) by substituting R_B with $R_{B,m}$. This improvement is further highlighted by Figure 8-right, which reports the distribution of the percentage error on the validation set. The error distribution obtained with the uncorrected Breguet formulation is mainly shifted toward positive values, confirming that the classical formulation tends to overestimate the cruise range when venting losses are neglected. Moreover, the distribution is relatively wide, meaning that the prediction error varies significantly across the investigated tank configurations. By contrast, the error distribution obtained with the modified Breguet formulation is much more concentrated around zero. This indicates that the surrogate correction not only reduces the average prediction error, but also limits the dispersion of the error over the validation set.

To quantify the results observed in Figure 8-right, the main accuracy indicators of the robustness of the proposed formulation are summarized in Table 5 for training set, validation set and the overall dataset. In particular, the mean absolute percentage error (MAPE) provides an average measure of the prediction accuracy, the root mean square percentage error (RMSPE) penalizes larger deviations, the BIAS error indicates whether the model tends to overestimate or underestimate the range, and the maximum absolute percentage error (MAXE) identifies the worst prediction in the validation set. The MAPE is computed by calculating the mean value of $|\Delta R|$ to the considered dataset, the RMSPE is computed through the root means square of ΔR, the bias is the mean value of ΔR, and MAXE is the maximum value of $|\Delta R|$ in the considered dataset. Quantitatively, in the validation set, the MAPE decreases from 0.93% to 0.32%, the RMSPE decreases from 2.43% to 0.43%, and the maximum absolute error is reduced from 13.68% to 1.62%. At the same time, the bias becomes almost negligible, showing that the corrected formulation does not introduce a systematic overprediction or underprediction of the range. Even slightly better results are obtained in case of training set and the overall dataset.

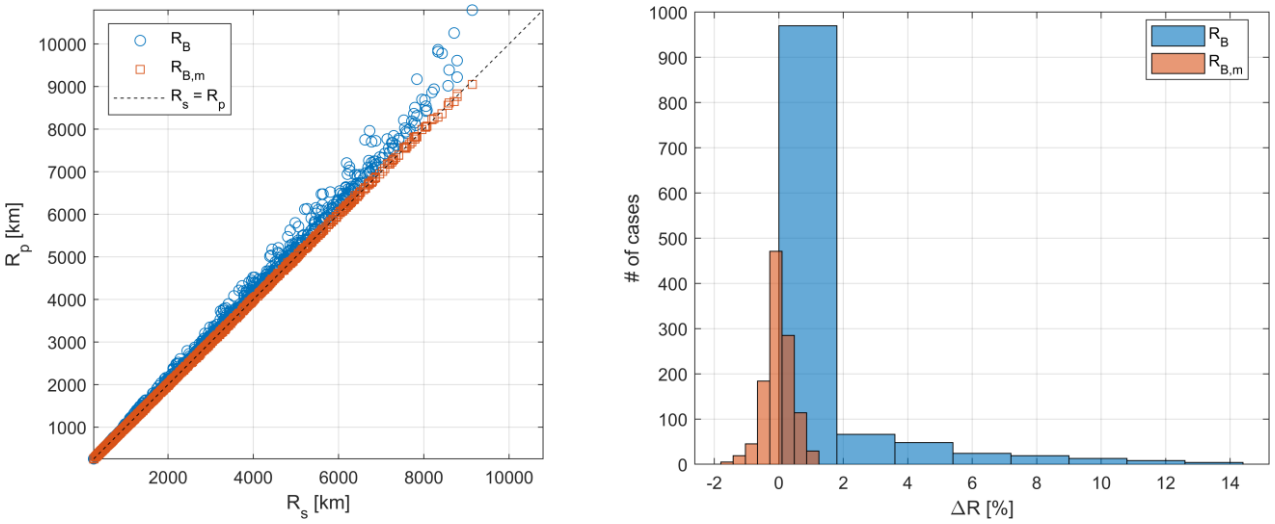


Figure 8 – Parity plot of predicted range vs simulated range (left), and histograms comparing the error between predicted range and simulated range.

Table 5 – Main accuracy indicators of the proposed formulation.

	Case 1	Case 2	Case 3	Case 4	Case 5	Case 6
DATASET	Training	Training	Validation	Validation	All dataset	All dataset
MODEL	R_B	$R_{B,m}$	R_B	$R_{B,m}$	R_B	$R_{B,m}$
MAPE [%]	1.12	0.34	0.93	0.32	1.09	0.33
RMSPE [%]	2.75	0.44	2.43	0.43	2.69	0.43
BIAS [%]	1.13	0.01	0.93	-0.01	1.09	0.007
MAXE [%]	13.56	1.76	13.68	1.62	13.68	1.76

4. Conclusion

This work proposed a novel Breguet formulation for liquid-hydrogen-powered aircraft, aimed at preserving the simplicity and physical interpretability of the classical Breguet equation while introducing the effect of cryogenic storage losses. The formulation was derived from a coupled mission-tank simulation framework in which the aircraft cruise performance and the thermodynamic evolution of the liquid-hydrogen tank were advanced simultaneously in time. The tank model accounted for heat ingress, boil-off, ullage pressure rise, and venting, allowing the initial hydrogen mass stored in the tank to be distinguished from the hydrogen mass effectively available for propulsion.

To correct the analytical range estimate, a power-law logarithmic surrogate with interaction terms was calibrated using a database of 5760 tank configurations obtained by varying five design variables: tank length, tank radius, insulation thickness, venting pressure, and initial fill factor. The dataset was divided into a calibration set of 4608 configurations and a validation set of 1152 configurations. The calibration set was used to solve an optimization problem aimed at identifying the optimal surrogate coefficients by minimizing the mean squared relative error between the modified Breguet range and the coupled mission-tank simulation results, while the remaining configurations were retained only to assess the predictive capability of the formulation. On the validation set, the mean absolute percentage error decreased from 1.12% for the uncorrected Breguet formulation to 0.32% for the modified formulation, while the maximum absolute error was reduced from 13.68% to 1.62% and the bias became almost negligible. Similar results were obtained on the training set and on the complete dataset, confirming the robustness of the proposed correction within the investigated design space.

To have a comprehensive overview of the effect of the tank size on the aircraft range, a parametric analysis has been carried out. It showed that increasing insulation thickness reduced heat ingress and therefore decreased the amount of vented hydrogen. However, thicker insulation also reduced

the internal volume available for liquid hydrogen storage, leading in many configurations to a slight reduction in cruise range. Increasing tank length and radius generally increased the simulated range because of the larger amount of hydrogen stored onboard, but it also increased the cumulative vented mass, mainly because longer missions allow venting losses to accumulate over a longer time. Increasing venting pressure reduced the vented mass by delaying gas discharge, although this benefit was partly counterbalanced by the higher structural mass required by the larger design pressure. This same coupling between storage thermodynamics and aircraft-level performance is also reflected in the comparison between the coupled mission simulations and the well-known Breguet formula, which showed that neglecting boil-off and venting leads to a systematic overprediction of cruise range. The introduction of the Propulsive Energy Utilization Factor Ψ, proposed here as a new metric for liquid-hydrogen aircraft which also showed that improving the thermodynamic efficiency of the storage system does not automatically maximize aircraft range. Configurations with lower venting losses may require heavier structures or reduced storage volume, so the final aircraft design must balance range capability, gravimetric efficiency, and energy utilization.

The proposed formulation represents a compact and computationally efficient tool for preliminary sizing and trade-off studies of liquid-hydrogen aircraft. It does not replace detailed mission and tank simulations, but it provides a practical analytical correction that can be used during early design phases, when many configurations must be evaluated rapidly. Future developments will extend the formulation to the complete mission profile, including climb, descent, reserve segments, and ground operations. Additional work should also consider different tank layouts, center-of-gravity effects and validation against higher-fidelity cryogenic tank models or experimental data. These extensions will further improve the applicability of the proposed Breguet-based formulation to the conceptual design and optimization of future hydrogen-powered aircraft.

5. Contact Author Email Address

The corresponding author is Karim Abu Salem, mailto: karim.abusalem@unitn.it

6. Copyright Statement

The authors confirm that they, and/or their company or organization, hold copyright on all of the original material included in this paper. The authors also confirm that they have obtained permission, from the copyright holder of any third party material included in this paper, to publish it as part of their paper. The authors confirm that they give permission, or have obtained permission from the copyright holder of this paper, for the publication and distribution of this paper as part of the ICAS proceedings or as individual off-prints from the proceedings.

References

[1] Ficca A, Marulo F and Sollo A. An open thinking for a vision on sustainable green aviation. *Progress in Aerospace Sciences*, Vol. 141, 2023. https://doi.org/10.1016/j.paerosci.2023.100928

[2] Afonso F, et al. Strategies towards a more sustainable aviation: A systematic review. *Progress in Aerospace Sciences*, Vol. 137, 2023. https://doi.org/10.1016/j.paerosci.2022.100878

[3] Delbecq S, et al. Sustainable aviation in the context of the Paris Agreement: A review of prospective scenarios and their technological mitigation levers. *Progress in Aerospace Sciences*, Vol. 141, 2023. https://doi.org/10.1016/j.paerosci.2023.100920

[4] Platzer MF. The prospects for green aviation by 2050. *Progress in Aerospace Sciences*, Vol. 141, 2023. https://doi.org/10.1016/j.paerosci.2023.100926

[5] Cardone LM, Petrone G, De Rosa S, et al. Review of the recent developments about the hybrid propelled aircraft. *Aerotecnica Missili & Spazio*, Vol. 103, pp 17-37, 2024. https://doi.org/10.1007/s42496-023-00173-6

[6] Carrera E, Palaia G and Abu Salem K. The green transition in commercial aviation. *Rendiconti Lincei. Scienze Fisiche e Naturali*, Vol. 36, pp 785-829, 2025. https://doi.org/10.1007/s12210-025-01345-1

[7] Khandelwal B. Hydrogen powered aircraft: The future of air transport. *Progress in Aerospace Sciences*, Vol. 60, pp 45-59, 2013. http://dx.doi.org/10.1016/j.paerosci.2012.12.002

[8] Dincer I and Acar C. A review on potential use of hydrogen in aviation applications. *International Journal of Sustainable Aviation*, Vol. 2, No. 1, pp 74-100, 2016. https://doi.org/10.1504/IJSA.2016.076077

[9] Bicer Y and Dincer I. Life cycle evaluation of hydrogen and other potential fuels for aircrafts. *International Journal of Hydrogen Energy*, Vol. 42, 2017. https://doi.org/10.1016/j.ijhydene.2016.12.119

[10]Baroutaji A, Wilberforce T, Ramadan M and Olabi A G. Comprehensive investigation on hydrogen and fuel cell technology in the aviation and aerospace sectors. *Renewable and Sustainable Energy Reviews*, Vol. 106, pp 31-40, 2019. https://doi.org/10.1016/j.rser.2019.02.022

[11]Prewitz M, Bardenhagen A and Beck R. Hydrogen as the fuel of the future in aircrafts - Challenges and opportunities. *International Journal of Hydrogen Energy*, Vol. 45, No. 46, pp 25378-25385, 2020. https://doi.org/10.1016/j.ijhydene.2020.06.238

[12]Manigandan S, Praveenkumar T R, Ryu J I, Verma T N and Pugazhendhi A. Role of hydrogen on aviation sector: A review on hydrogen storage, fuel flexibility, flame stability, and emissions reduction on gas turbines engines. *Fuel*, Vol. 352, 129064, 2023. https://doi.org/10.1016/j.fuel.2023.129064

[13]Adler EJ and Martins JRRA. Hydrogen-powered aircraft: Fundamental concepts, key technologies, and environmental impacts. *Progress in Aerospace Sciences*, Vol. 141, 2023. https://doi.org/10.1016/j.paerosci.2023.100922

[14]Tiwari S, Pekris M J and Doherty JJ. A review of liquid hydrogen aircraft and propulsion technologies. *International Journal of Hydrogen Energy*, Vol. 57, pp 1174-1196, 2024. https://doi.org/10.1016/j.ijhydene.2023.12.263

[15]Boretti A. Towards hydrogen gas turbine engines aviation: A review of production, infrastructure, storage, aircraft design and combustion technologies. *International Journal of Hydrogen Energy*, Vol. 88, pp 279-288, 2024. https://doi.org/10.1016/j.ijhydene.2024.09.121

[16]Soleymani M, Mostafavi V, Hebert M, Kelouwani S and Boulon L. Hydrogen propulsion systems for aircraft, a review on recent advances and ongoing challenges. *International Journal of Hydrogen Energy*, Vol. 91, pp 137-171, 2024. https://doi.org/10.1016/j.ijhydene.2024.10.131

[17]Leitão ABV, Bringhenti C, Tomita J T, dos Santos Silva F J, Xisto C and Grönstedt T. A review of hydrogen aircraft propulsion systems: recent advances and environmental perspectives., *International Journal of Hydrogen Energy*, Vol. 176, 151489, 2025. https://doi.org/10.1016/j.ijhydene.2025.151489

[18]Gopalasingam D, Rakhshani B and Rodriguez C. Hydrogen propulsion technologies for aviation: A review of fuel cell and direct combustion systems towards decarbonising medium-haul aircraft. *Hydrogen*, Vol. 6, No. 4, 92, 2025. https://doi.org/10.3390/hydrogen6040092

[19]Nojoumi H, Dincer I and Naterer GF. Greenhouse gas emissions assessment of hydrogen and kerosene-fueled aircraft propulsion. *International Journal of Hydrogen Energy*, Vol. 34, 2009. https://doi.org/10.1016/j.ijhydene.2008.11.017

[20]Verstraete D, Hendrick P, Pilidis P and Ramsden K. Hydrogen fuel tanks for subsonic transport aircraft. *International Journal of Hydrogen Energy*, Vol. 35, 2010. https://doi.org/10.1016/j.ijhydene.2010.06.060

[21]Verstraete D. Long range transport aircraft using hydrogen fuel. *International Journal of Hydrogen Energy*, Vol. 38, 2013. https://doi.org/10.1016/j.ijhydene.2013.09.021

[22]Verstraete D. On the energy efficiency of hydrogen-fuelled transport aircraft. *International Journal of Hydrogen Energy*, Vol. 40, 2015. https://doi.org/10.1016/j.ijhydene.2015.04.055

[23]Onorato G, Proesmans P and Hoogreef MFM. Assessment of hydrogen transport aircraft. *CEAS Aeronautical Journal*, Vol. 13, pp 813-845, 2022. https://doi.org/10.1007/s13272-022-00601-6

[24]Jagtap SS, et al. Performance sensitivity of subsonic liquid hydrogen long-range tube-wing aircraft to technology developments. *International Journal of Hydrogen Energy*, Vol. 50, pp 820-833, 2024.

[25]Proesmans P and Vos R. Hydrogen, medium-range airplane design optimization for minimal global warming impact. *CEAS Aeronautical Journal*, Vol. 15, pp 781-806, 2024. https://doi.org/10.1007/s13272-024-00734-w

[26]Grazioso G, De Marco A, Della Vecchia P, Di Stasio M, Trifari V, Nicolosi F. A simulation-based mission optimization approach for regional transport hybrid-electric aircraft. *Applied Energy*, Vol. 402. https://doi.org/10.1016/j.apenergy.2025.126869

[27]Karpuk S, Ma Y and Elham A. Design investigation of potential long-range hydrogen combustion blended wing body aircraft with future technologies. *Aerospace*, Vol. 10, No. 6, 566, 2023. https://doi.org/10.3390/aerospace10060566

[28]Jagtap SS, et al. Conceptual design-optimisation of a subsonic hydrogen-powered long-range blended-wing-body aircraft. *International Journal of Hydrogen Energy*, Vol. 96, pp 639-651, 2024. https://doi.org/10.1016/j.ijhydene.2024.11.331

[29]Thomas B and Agarwal RK. Evaluation of sustainable transonic truss-braced wing aircraft configurations using liquid hydrogen fuel. *AIAA SCITECH 2023 Forum*, National Harbor, MD & Online, 23-27 January 2023, AIAA 2023-2175. https://doi.org/10.2514/6.2023-2175

[30]Wahler NFM, Ma Y and Elham A. Conceptual design and aerostructural trade-offs in hydrogen-powered strut-braced wing aircraft: Insights into dry and wet ultra-high aspect ratio wings. *Aerospace*, Vol. 12, No. 2, 77, 2025. https://doi.org/10.3390/aerospace12020077

[31]Palaia G, Abu Salem K and Carrera E. Preliminary performance analysis of medium-range liquid hydrogen-powered box-wing aircraft. *Aerospace*, Vol. 11, No. 5, 379, 2024.

https://doi.org/10.3390/aerospace11050379

[32]Cipolla V, Zanetti D, Abu Salem K, Binante V and Palaia G. A parametric approach for conceptual integration and performance studies of liquid hydrogen short-medium range aircraft. *Applied Sciences*, Vol. 12, No. 14, 6857, 2022. https://doi.org/10.3390/app12146857

[33]Abu Salem K, Palaia G, Frediani A and Carrera E. The box-wing configuration: a critical review of design approaches and applications. *Progress in Aerospace Sciences*, Vol. 157, 2025. https://doi.org/10.1016/j.paerosci.2025.101108

[34]Bagarello S, Campagna D and Benedetti I. A survey on hydrogen tanks for sustainable aviation. *Green Energy and Intelligent Transportation*, 2024. https://doi.org/10.1016/j.geits.2024.100224

[35]Mital SK, Gyekenyesi JZ, Arnold SM, Sullivan RM, Manderscheid JM and Murthy PLN. Review of current state of the art and key design issues with potential solutions for liquid hydrogen cryogenic storage tank structures for aircraft applications. NASA Technical Reports Server ID: 20060056194, 2006. https://ntrs.nasa.gov/citations/20060056194

[36]Magliano A, Perez Carrera C, Pappalardo CM, Guida D and Berardi VP. A comprehensive literature review on hydrogen tanks: Storage, safety, and structural integrity. *Applied Sciences*, Vol. 14, No. 20, 9348, 2024. https://doi.org/10.3390/app14209348

[37]Wang HR, et al. Modeling and thermodynamic analysis of thermal performance in self-pressurized liquid hydrogen tanks. *International Journal of Hydrogen Energy*, Vol. 47, No. 71, pp 30530-30545, 2022. https://doi.org/10.1016/j.ijhydene.2022.07.027

[38]Adler EJ and Martins JRRA. Liquid hydrogen tank boil-off model for design and optimization. *Journal of Thermophysics and Heat Transfer*, Vol. 39, 2025. https://doi.org/10.2514/1.T7005

[39]Winnefeld C, Kadyk T, Bensmann B, Krewer U and Hanke-Rauschenbach R. Modelling and designing cryogenic hydrogen tanks for future aircraft applications. *Energies*, Vol. 11, 105, 2018. https://doi.org/10.3390/en11010105

[40]Al Ghafri SZS, Swanger A, Jusko V, Siahvashi A, Perez F, Johns ML and May EF. Modelling of liquid hydrogen boil-off. *Energies*, Vol. 15, 1149, 2022. https://doi.org/10.3390/en15031149

[41]Mantzaroudis VK and Theotokoglou EE. Computational analysis of liquid hydrogen storage tanks for aircraft applications. *Materials*, Vol. 16, No. 6, 2245, 2023. https://doi.org/10.3390/ma16062245

[42]Mazzoni F, Biga R, Manrique-Escobar CA, Brusa E and Delprete C. Design space exploration through liquid H2 tank preliminary sizing and design of experiments analysis. *International Journal of Hydrogen Energy*, Vol. 95, pp 1252-1260, 2024. https://doi.org/10.1016/j.ijhydene.2024.08.017

[43]Oliet C, Mosqueda-Otero M, Schillaci E, Amani A, Rigola J and Castro J. Thermal digital twin of LH2 aircraft storage tank. *Engineering Proceedings*, Vol. 90, 97, 2025. https://doi.org/10.3390/engproc2025090097

[44]Appel KR, Matveev KI and Leachman JW. Modeling the effects of liquid hydrogen tank operations on boil-off losses. *Cryogenics*, Vol. 150, 104161, 2025. https://doi.org/10.1016/j.cryogenics.2025.104161

[45]Fernandes S, Korsukova EV, Ellis CD, Ambrose S and Eastwick CN. A CFD comparison of interfacial phase change models for boil-off, self-pressurisation and thermal stratification in liquid hydrogen storage tanks. *International Journal of Heat and Mass Transfer*, Vol. 256, 128067, 2026. https://doi.org/10.1016/j.ijheatmasstransfer.2025.128067

[46]Kangwanpongpan T, Makarov D, Cirrone D and Molkov V. LES model of flash-boiling and pressure recovery phenomena during release from large-scale pressurised liquid hydrogen storage tank. *International Journal of Hydrogen Energy*, Vol. 50, pp 390-405, 2024. https://doi.org/10.1016/j.ijhydene.2023.07.126

[47]Middha P, Ichard M and Arntzen B J. Validation of CFD modelling of LH2 spread and evaporation against large-scale spill experiments. *International Journal of Hydrogen Energy*, Vol. 36, pp 2620-2627, 2011. https://doi.org/10.1016/j.ijhydene.2010.03.122

[48]Risse K, Schäfer K, Schültke F and Stumpf E. Central reference aircraft data system (CeRAS) for research community. *CEAS Aeronautical Journal*, Vol. 7, No. 1, pp 121-133, 2016. DOI: 10.1007/s13272-015-0177-9

[49]Abu Salem K, Cipolla V, Palaia G, Binante V and Zanetti D. A physics-based multidisciplinary approach for the preliminary design and performance analysis of a medium range aircraft with box-wing architecture. *Aerospace*, Vol. 8, No. 10, 292, 2021. https://doi.org/10.3390/aerospace8100292

[50]Tzoumakis G, Fotopoulos K and Lampeas G. Multi-physics digital model of an Aluminum 2219 liquid hydrogen aircraft tank. *Aerospace*, Vol. 11, No. 2, 161, 2024. https://doi.org/10.3390/aerospace11020161

[51]Brewer GD, Morris RE, Lange RH and Moore JW. Study of the application of hydrogen fuel to long-range subsonic transport aircraft. Volume 1: Summary. NASA Contractor Report NASA-CR-132558, 1975.

[52]Brewer GD. The prospects for liquid hydrogen fueled aircraft. *International Journal of Hydrogen Energy*, Vol. 7, No. 1, pp 21-41, 1982. https://doi.org/10.1016/0360-3199(82)90205-1

[53]American Society of Mechanical Engineers. ASME Boiler and Pressure Vessel Code, Rules for

Construction of Pressure Vessels (Alternative Rules). Section VIII, Division 2; American Society of Mechanical Engineers: New York, NY, USA, 2017.

[54]Burschyk T, Cabac Y, Silberhorn D, Boden B and Nagel B. Liquid hydrogen storage design trades for a short-range aircraft concept. *CEAS Aeronautical Journal*, Vol. 14, pp 879-893, 2023. https://doi.org/10.1007/s13272-023-00689-4

[55]Corchero G and Montañés JL. An approach to the use of hydrogen for commercial aircraft engines. Proceedings of the Institution of Mechanical Engineers, *Part G: Journal of Aerospace Engineering*, Vol. 219, No. 1, pp 35–44, 2005. DOI: 10.1243/095441005X9139.